

Searching for the pulsar in G18.95–1.1: Discovery of an X-ray point source and associated synchrotron nebula with Chandra

R. Tüllmann¹, P. P. Plucinsky¹, T. J. Gaetz¹, P. Slane¹, J. P. Hughes², I. Harrus^{3,*}, and T. G. Pannuti⁴

ABSTRACT

Using the *Chandra* X-ray Observatory, we have pinpointed the location of a faint X-ray point source (CXOU J182913.1-125113) and an associated diffuse nebula in the composite supernova remnant G18.95-1.1. These objects appear to be the long-sought pulsar and its wind nebula. The X-ray spectrum of the point source is best described by an absorbed powerlaw model with $\Gamma = 1.6$ and an N_H of $\sim 1 \times 10^{22} \text{ cm}^{-2}$. This model predicts a relatively low unabsorbed X-ray luminosity of about $L_X(0.5 - 8.0 \text{ keV}) \simeq 4.1 \times 10^{31} D_2^2 \text{ erg s}^{-1}$, where D_2 is the distance in units of 2kpc. The best-fitted model of the diffuse nebula is a combination of thermal ($kT = 0.48 \text{ keV}$) and non-thermal ($1.4 \leq \Gamma \leq 1.9$) emission. The unabsorbed X-ray luminosity of $L_X \simeq 5.4 \times 10^{33} D_2^2 \text{ erg s}^{-1}$ in the 0.5–8keV energy band seems to be largely dominated by the thermal component from the SNR, providing 87% of L_X in this band. No radio or X-ray pulsations have been reported for CXOU J182913.1-125113. If we assume an age of $\sim 5300 \text{ yr}$ for G18.95-1.1 and use the X-ray luminosity for the pulsar and the wind nebula together with the relationship between spin-down luminosity (via magnetic dipole radiation) and period, we estimate the pulsar's period to be $P \simeq 0.4 \text{ s}$. Compared to other rotation-powered pulsars, a magnetic field of $2.2 \times 10^{13} \text{ G}$ is implied by its location in the $P-\dot{P}$ diagram, a value which is close to that of the quantum critical field.

Subject headings: ISM: supernova remnants — (stars:) pulsars: general — X-rays: individual (G18.95-1.1)

1. Introduction

Supernova remnants (SNRs) with a center-filled or composite morphology often host young pulsars whose strong relativistic winds can lead to the formation of pulsar wind nebulae (PWNe). In recent years the high spatial resolution of *Chandra* has made it possible to detect the PWNe, to pinpoint the locations of the compact objects, and to constrain their nature. A new, yet un-

proven, case in which a putative pulsar is suspected to power a PWN is G18.95–1.1. For this composite SNR, which is considered to be located in the Sagittarius Arm at a distance of $\sim 2 \text{ kpc}$ (Fürst et al. 1989), an X-ray luminosity of $6.1 \times 10^{34} \text{ erg s}^{-1}$ (0.1–10 keV) has been reported by Harrus et al. (2004). G18.95–1.1 was discovered as a shell-like non-thermal extended radio source (Reich et al. 1984). Further observations carried out at GHz frequencies by Fürst et al. (1985), Odegard (1986), and Fürst et al. (1997) detected an elongated synchrotron nebula in the center of G18.95–1.1 and a region of enhanced radio emission at its tip, much like the central PWN in W44 (e.g., Petre et al. 2002). Another region of enhanced radio emission is located along the western shell of G18.95–1.1. The age of the remnant and its radio diameter are considered to be (4.4–

¹Harvard-Smithsonian Center for Astrophysics, 60 Garden Street, Cambridge, MA 02138; rtuellmann@cfa.harvard.edu

²Department of Physics and Astronomy, Rutgers University, 136 Frelinghuysen Road, Piscataway, NJ 08854

³NASA/GSFC

*Currently at NASA HQ, Washington DC

⁴Space Science Center, 235 Martindale Drive, Morehead State University, Morehead, KY 40351

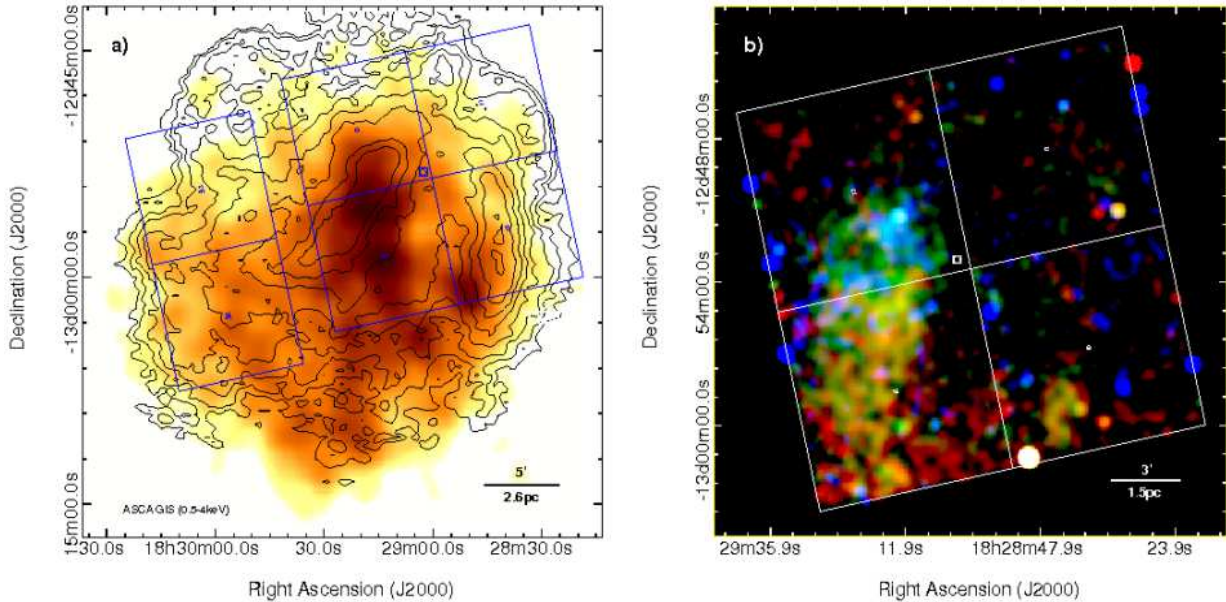


Fig. 1.— a): X-ray image of G18.95–1.1 obtained with the *ASCA* GIS ($FWHM=45''$) in the 0.5–4keV energy band and overlaid with 10.55GHz radio continuum contours and the ACIS-I FOV. b): Exposure-corrected multi-color X-ray image of the inner part of G18.95–1.1 (red = 0.35–1.1 keV, green = 1.1–2.6 keV, blue = 2.6–8.0 keV). The image has been binned by a factor of 8 and smoothed with a Gaussian kernel of $FWHM = 6$ pix.

6.1×10^3 yr (Harrus et al. 2004) and $\sim 33'$ (e.g., Odegard 1986; Patnaik et al. 1988; Fürst et al. 1989) which is equivalent to $\sim 18D_2$ pc, where D_2 is the distance in units of 2kpc.

In a previous X-ray study carried out with *ROSAT* and *ASCA*, Harrus et al. (2004) mapped the diffuse X-ray emission of G18.95–1.1. A reproduction of the *ASCA* image in the 0.5–4keV energy band is shown in Fig. 1a together with radio contours at 10.55GHz (Fürst et al. 1997). The radio emission consists of a central elongated radio-bright nebula ($L_{10^7-10^{11}\text{Hz}} = 5 \times 10^{33}$ erg s^{-1} , Fürst et al. 1989) running from the NW to the SE and another region of enhanced radio emission located at the western shell of G18.95–1.1. Harrus et al. (2004) also detected a localized region of hard X-ray emission in the 4–10keV energy band whose peak emission is centered at RA= $18^{\text{h}}29^{\text{m}}03^{\text{s}}.3$, Dec= $-12^{\circ}52'58''.9$ (see also their Fig. 2 for its location). This hard X-ray emission is slightly offset from the region of enhanced radio synchrotron emission, similar to G326.3–1.8 (Plucinsky et al. 2002). Harrus et al. found that the X-ray emission from G18.95–1.1 is

predominantly thermal, heavily absorbed with a column density of about 1×10^{22} cm^{-2} , and can be best described by a non-equilibrium ionization (NEI) model with a temperature of ~ 0.9 keV and an ionization timescale of 1.3×10^{10} cm^{-3} s^{-1} . In a reanalysis of the *ASCA* data of the localized hard X-ray emission, we confirmed the existence of a non-thermal component, which seems to dominate the spectrum above 2 keV. Although *ASCA*'s spatial resolution is insufficient to detect a point source within this region, it is possible that the hard X-ray emission indicates the location of an undetected pulsar.

We have learned from *Chandra* observations that many young pulsars, like those in 3C 58 and G21.5-0.9 as well as currently undetected pulsars, e.g., the one in G327.1-1.1, are embedded in extended non-thermal emission from the PWNe. In the case of G18.95–1.1 the extended emission is most likely also contaminated by diffuse thermal emission from the SNR, but any non-thermal emission from a possible point source remained unresolved by *ASCA*. With *Chandra* we now have the opportunity to detect a point source in this

extended emission. Therefore, we conducted a follow-up *Chandra* observation of G18.95-1.1 in order to search for an X-ray point source embedded in the extended emission, to determine its nature, and to characterize the spatial and spectral distribution of the hard emission to test if it is consistent with an X-ray synchrotron nebula.

2. Follow-up *Chandra* Observations

A 45 ks *Chandra* observation was executed on August 3rd, 2009 (ObsID 10098) using ACIS-I in *vfaint* mode with the aimpoint of the ACIS-I array centered onto the region in which the 4–10 keV emission from *ASCA* overlapped the radio synchrotron emission (see Fig. 1a). Data reduction was carried out with CIAO 4.2 and CALDB version 4.2.2, following standard procedures¹, except for the charge transfer inefficiency (CTI) correction. As during the last 11ks of the observation the focal plane temperature was warmer than -118.7C (increasing from -119.0C to -118.4C), we applied a time-dependent CTI correction following Posson-Brown et al. (2010). The effects of this correction are marginal in the 0.35–8.0 keV energy band as it adjusted the gain on average by $\sim 0.5\%$ to account for the increased CTI at higher temperatures.

3. Data Analysis

In Fig. 1b we show the high-resolution *Chandra* X-ray composite image of the inner part of G18.95-1.1. It reveals a region of hard X-ray emission at RA=18^h29^m13^s.1, Dec=-12°51'13".4 ($l=+18^{\circ}58'58''.4$, $b=-00^{\circ}59'59''.1$), which is shown in greater detail in Fig. 2. This hard emission seems to originate from a point-like source and its immediate vicinity (its extent corresponds to region e1 highlighted in Fig. 2). The point-like source is located at the northern tip of a trail of softer diffuse X-ray emission extending towards the SE and pointing back towards the center of the remnant. The extended emission is well aligned with the radio synchrotron nebula, but does not appear to cover the full extent of the latter (see red contours in Fig. 2).

Comparing the radial profile of this source with the one from an SAOTrace simulation, confirmed

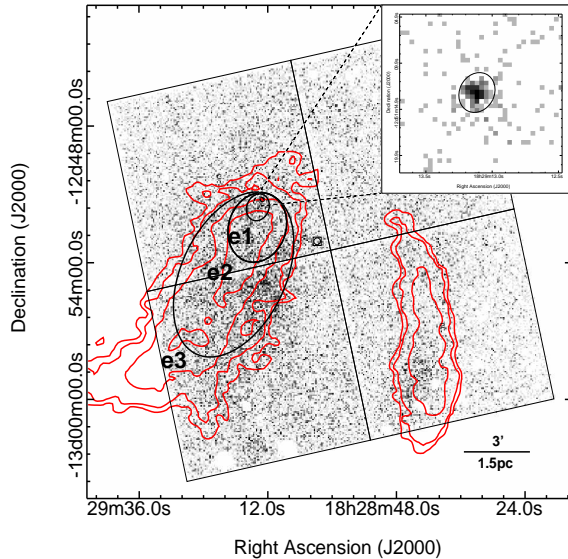


Fig. 2.— 10.55GHz radio continuum contours (Fürst et al. 1997) overlaid onto a *Chandra* counts image (bin=8, 0.35–2.6keV, point source-subtracted). The inlay shows the unbinned counts image of the point source in the full band and a SAOTrace simulation of the PSF (90% encircled energy). Both images are displayed on a square root scale and plotted between 0 and 12 counts pix^{-1} . Spectral extraction regions are shown as black ellipses.

that this source is indeed a point source. This object, CXOU J182913.1-125113 hereafter, is the only X-ray point source detected within a circle of 1'.4 radius centered on the position of the source. CXOU J182913.1-125113 has no known radio, 2MASS, optical, or γ -ray counterpart.

The brightest point source in the field (the bright white object near the southern edge of the FOV in Fig. 1b) was classified by Harrus et al. (2004) as a late-type star and appears not to be associated with G18.95-1.1. There are other sources in the field which could be pulsar candidates, notably the pair of sources near RA = 18^h28^m36^s.0, Dec = -12°51'00".8 ($l=+18^{\circ}54'57''.4$, $b=-00^{\circ}51'52''.0$). However, these sources have soft X-ray spectra as indicated by their colors in Fig. 1b, are $\sim 8.0'$ away from the diffuse nebula, and can be associated with foreground stars in the USNO-b1.0 catalog (Monet et al. 2003). The other point-like objects in the field which appear on or outside

¹http://exc.harvard.edu/ciao/guides/acis_data.html

the edge of the FOV are most likely artifacts of the smoothing in regions with low and/or variable exposure. In addition, faint enhancements in the diffuse emission or in the background might appear to be point-like after smoothing.

Although the searches for pulsations in the radio by Fürst et al. (1989) proved unsuccessful (their closest search position is $\sim 3'4$ away from CXOU J182913.1-125113), the coincidence of the X-ray and radio synchrotron emission as well as the cometary-shaped morphology of the diffuse X-ray emission, with a hard X-ray point source at the tip, seems to point at a pulsar and its wind nebula.

To test if the point source and the extended emission are consistent with this interpretation, we extracted spectra for the putative pulsar and from three extended regions to the south of this source, using the CIAO tool `specextract`. For the putative pulsar we extracted all counts within a radius of $5''.2$, while the three elliptical extraction regions shown in Fig. 2 were used for the extended emission from which only the point source was excluded. Two additional spectra were extracted which cover different fractions of the extended X-ray emission. They contain all counts in the e2 – e1 and e3 – e2 regions. This approach was chosen because we wanted to see how the spectra and the X-ray luminosity change as a function of increasing distance from the pulsar candidate. Background for the pulsar candidate was taken from an annular region centered on the position of this source and from regions close to the ACIS chip edges for the extended X-ray emission. All spectra were grouped with `dmgroup` until at least a signal-to-noise ratio of 3 (5) was achieved for the pulsar candidate (extended sources).

3.1. The X-ray Point Source

The spectrum labeled 'ps' in Fig. 3 shows the X-ray emission from the point source. It contains 168 net counts and was fitted in `XSPEC` (v12.6.0) with an absorbed powerlaw model and alternatively with an absorbed thermal plasma model. To simulate the absorption the `tbabs` model (Wilms et al. 2000) was used while the thermal emission was modeled with the `apec` model (Smith et al. 2001). The N_H was allowed to vary, but was initially set to the Galactic value of $N_H = (1.3 \pm 0.4) \times 10^{22} \text{ cm}^{-2}$ (Dickey & Lockman 1990).

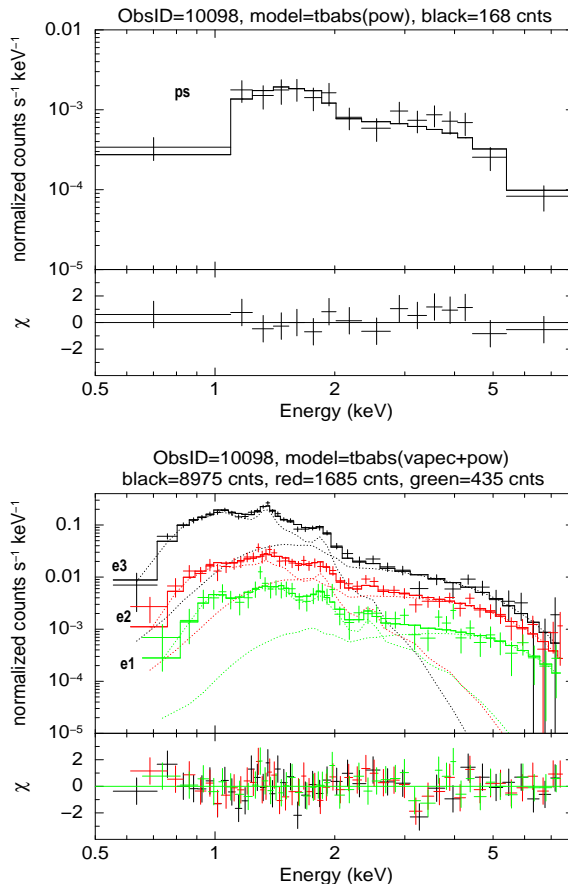


Fig. 3.— Top: Best-fitted powerlaw model for the point source (ps). Bottom: Spectra extracted from regions e1 to e3 can be best fitted by a combination of a *vapec* model and a powerlaw.

The best-fitted model ($\chi^2/\nu = 12.87/35 = 0.37$) is the absorbed powerlaw with a photon index of $\Gamma = 1.6^{+0.4}_{-0.4}$ and an $N_H = 9.5^{+6.5}_{-4.7} \times 10^{21} \text{ cm}^{-2}$ (all uncertainties are given for a 90% confidence level). The predicted N_H is in good agreement with previous measurements from Fürst et al. (1997) and Harrus et al. (2004). Although the thermal plasma model provides an equally good fit, the predicted kT of 16keV is unreasonably high and therefore makes a thermal nature of the source very unlikely. The unabsorbed X-ray luminosities predicted by the powerlaw model in the 0.5–8.0keV and 2.0–8.0keV energy bands amount to $4.08^{+3.32}_{-1.00} \times 10^{31} D_2^2 \text{ erg s}^{-1}$ and $2.12^{+2.68}_{-1.40} \times 10^{31} D_2^2 \text{ erg s}^{-1}$, respectively.

TABLE 1
BEST-FIT RESULTS FOR THE PURELY DIFFUSE EMISSION

region (1)	χ_{red}^2/ν (2)	P value (3)	K_1 (4)	K_2 (5)	N_{H} (6)	kT_1 (7)	Γ (8)	$L_{0.5-8}$ (9)	$L_{2.0-8.0}$ (10)
e1	0.81/44	9.21E-01	4.74E-04	2.13E-05	$1.97_{-0.56}^{+0.52}$	0.48 (frozen)	$1.4_{-0.6}^{+0.2}$	$3.72_{-0.24}^{+0.54}$	$0.60_{-0.12}^{+0.36}$
e2	0.71/47	9.11E-01	4.53E-04	1.62E-04	$1.56_{-0.64}^{+0.36}$	0.48 (frozen)	$1.9_{-0.4}^{+0.3}$	$9.36_{-1.60}^{+2.32}$	$1.76_{-1.12}^{+1.56}$
e3	0.91/35	6.22E-01	7.31E-03	2.45E-04	$1.33_{-0.13}^{+0.12}$	$0.48_{-0.12}^{+0.06}$	$1.8_{-1.0}^{+0.6}$	$54.4_{-4.9}^{+8.7}$	$4.40_{-0.92}^{+4.32}$
e2-e1	0.82/47	8.04E-01	1.20E-03	7.23E-05	$1.54_{-0.32}^{+0.25}$	0.48 (frozen)	$1.7_{-0.4}^{+0.4}$	$9.68_{-0.84}^{+1.88}$	$1.28_{-0.20}^{+1.24}$
e3-e2	1.59/22	3.90E-02	5.35E-03	1.31E-04	$1.30_{-0.14}^{+0.12}$	$0.46_{-0.15}^{+0.06}$	$1.9_{-1.1}^{+1.4}$	$37.5_{-3.4}^{+5.2}$	$2.12_{-0.40}^{+2.16}$

(1): Extraction regions as shown in Fig. 2. (2): Reduced χ^2 of the best fit/degrees of freedom. (3): Assuming that the model is a good fit to the data, the P value is the probability of getting a χ^2 which is greater than the observed one. (4) and (5): $K_{1,2}$ are the normalization constants of the additive model components in units of cm^{-5} for K_1 (*vapec*) and photons $\text{keV}^{-1} \text{cm}^{-2} \text{s}^{-1}$ at 1 keV for K_2 (*pow*). (6): HI column density in units of 10^{22}cm^{-2} . (7): Temperature of the thermal plasma component. (8): Photon index. (9) and (10): Unabsorbed X-ray luminosities in units of 10^{32}ergs^{-1} .

The powerlaw index of 1.6 is consistent with the pulsar hypothesis and the derived luminosity is towards the low end of the distribution of pulsar luminosities. This may not be surprising since the brighter objects have already been discovered.

Under the simplistic assumption that the stellar remnant traverses the distance from the geometric center of the SNR (to be assumed at RA=18^h29^m23^s.9, Dec=-12°59′05″.1 or equivalently $l=+18^\circ 53' 13''.6$, $b=-01^\circ 05' 57''.7$) to its current location (4.3pc D_2^2) at a constant speed within 4400 to 6100 years, transverse velocities between 700 kms^{-1} and 960 kms^{-1} are estimated. Although these values are significantly higher than the typical ones of about 500 kms^{-1} (Gaensler & Slane 2006), they are not unusual for pulsars with periods significantly larger than several milliseconds (Toscano et al. 1999). A pulsar would be consistent with the derived spectral index from the powerlaw fit and the displacement between the radio synchrotron nebula and the X-ray point source.

3.2. The PWN candidate

The spectra of the purely diffuse X-ray emission extracted from regions e1, e2, and e3 are shown in the lower panel of Fig. 3 together with the best-fitted model (*tbabs(vapec + pow)*). Fitting the spectra with a single VNEI model (Borkowski et al. 2001) resulted in χ_{red}^2 values >2 , while a VNEI model with an additional component (e.g., *tbabs(vnei + pow)*) produced ionization timescales of $(2.3 \pm 1.1) \times 10^{13} \text{s cm}^{-3}$ which in-

dicate that the plasma is in collisional ionization equilibrium.

The spectrum labeled e3 covers the bulk of the extended X-ray emission near the center of G18.95-1.1. It has 8975 net counts and provides evidence of Mg XI emission around 1.35keV. The model predicts a thermal plasma temperature of 0.48keV and a photon index of $\Gamma = 1.8$. The best-fit results are shown in Table 1 and are given for a 90% confidence level. In case of e3, we freed the magnesium abundance to remove significant residuals around this line, yielding a relative Mg abundance of 1.4 ± 0.3 . This ratio is consistent with the Galactic value and agrees well with that reported by Harrus et al. (2004). The X-ray luminosities for e3 provide evidence that the gas is predominantly thermal, as 87% of L_X is emitted by the thermal plasma component in the 0.5–8keV energy band. The thermal emission could originate from the SNR’s shell seen along the line-of-sight or from the PWN if it has been disturbed by the reverse shock so that thermal emission and non-thermal emission are intertwined.

For e3, as well as for e1 and e2, the fitted HI column density is consistent with the average Galactic value of $(1.3 \pm 0.4) \times 10^{22} \text{cm}^{-2}$. A column that high seems to imply a distance much larger than 2kpc. However, as Fürst et al. (1989) and Harrus et al. (2004) argue, the alternative distance of 15kpc suggested by Fürst et al. (1989) appears unlikely, as the derived radio luminosity at this distance would be twice that of the Crab nebula, and the swept up mass of about

$3000M_{\odot}$ and the explosion energy of 2×10^{52} erg are unreasonably high. Even if we determine a distance based on the best-fit N_{H} , assuming $N_{\text{H}} = 1.3 \times 10^{-22} \text{ cm}^{-2}$ and an H I volume density of 0.4 cm^{-3} (Nakanishi & Sofue 2003), yielding a distance of about 11 kpc, the explosion energy of 9×10^{51} erg as well as the swept up mass of $\approx 1400 M_{\odot}$ are still unreasonably high. We therefore adopt a distance of 2 kpc for G18.95–1.1 and quote our results as a function of distance.

The Mg XI line emission seen in e3 remains undetected in the spectra for regions e2 and e1 (1685 and 435 net counts, respectively), but the bumps at about 1.87 keV indicate the presence of Si XIII emission and therefore a partly thermal origin of the gas. The photon index does not steepen significantly from e1 to e2 and the emission remains soft. For e1 73% and for e2 51% of the X-ray luminosity is produced by the thermal plasma component.

Fitting the spectra e1, e2, and e3 with only an absorbed powerlaw generally produces significantly worse fits ($0.78 \leq \chi_{red}^2 \leq 4.02$) with photon indices of $\Gamma = 1.9$ (e1), 2.2, (e2), and 3.9 (e3), respectively. Moreover, the potential emission features make a pure non-thermal origin of the X-ray emission appear very unlikely.

Because the pulsar and the PWN candidate are embedded within G18.95–1.1, the non-thermal emission from these objects is expected to be highly contaminated by the thermal emission from the SNR. We therefore adopt the temperature obtained from spectrum e3 to be representative for the inner part of G18.95–1.1 and freeze the kT for e1, e2, and e2–e1, respectively (see Table 1). This approach seemed to be justified, because spectra extracted from diffuse emission north of the pulsar candidate also suggested the kT to range from about 0.40 to 0.55 keV with relatively large uncertainties of 0.15 keV and N_{H} values which are consistent with those listed in Table 1.

For the extended X-ray emission to be consistent with a PWN, several criteria have to be met (see e.g. Safi-Harb 2004; Gaensler & Slane 2006). First, the X-ray surface brightness should decrease with increasing distance from the point source. Second, the radio spectral index α should be relatively flat ($0 \leq \alpha \leq 0.3$, $S_{\nu} \sim \nu^{-\alpha}$). Third, the photon index Γ should be steeper at X-ray energies than in the radio. As a consequence, the extent of the X-ray emission can be smaller than the extent

of the radio emission, as the synchrotron lifetime of the electrons in the X-ray regime can be shorter than those at radio wavelengths.

To test these criteria and to model how much the spectra change with increasing distance from the pulsar, we discuss spectra extracted from regions e1, e2–e1, and e3–e2 and focus on the hard, non-thermal X-ray emission emitted above 2 keV, which we solely attribute to the putative pulsar and the PWN. As can be seen from Table 1, the fraction of the X-ray luminosity above 2 keV decreases from 16% (e1), to 13% (e2–e1), down to 6% (e3–e2). If we take the hard X-ray luminosities and divide by the area of the extraction regions, we get surface brightnesses which decrease from $(1.77_{-0.35}^{+1.06}) \times 10^{28} D_2^2 \text{ erg s}^{-1} \text{ arcsec}^{-2}$ for e1, to $(6.60_{-0.35}^{+6.40}) \times 10^{27} D_2^2 \text{ erg s}^{-1} \text{ arcsec}^{-2}$ for e2–e1, down to $(2.64_{-0.05}^{+1.54}) \times 10^{27} D_2^2 \text{ erg s}^{-1} \text{ arcsec}^{-2}$ for e3–e2. Hence, the first criterion is fulfilled.

For the inner region of G18.95–1.1, flat radio spectral indices of $\alpha = 0.25 \pm 0.12$ (Odegard 1986) and $\alpha = 0.26 \pm 0.05$ (Fürst et al. 1989) have been reported. As the radio emission is also polarized in this region, Fürst et al. (1985) report an integrated polarization percentage of about 2.5% at 4.75 GHz for the whole remnant, the second criterion is met, too. The average photon index derived from the X-ray spectral fits is $\Gamma = 1.7_{-0.4}^{+0.5}$, significantly steeper than the radio index, thereby satisfying the third criterion. There is no significant steepening towards the edge of the nebula (see column 8, Table 1). We also fitted the spectra with the N_{H} fixed to the value of e3, but the uncertainties were still too large to say with any confidence that there is a clear trend in photon index. Furthermore, the major half-axis diameter of the X-ray emission in region e3 is about $7'.7$ ($\approx 4 \text{ pc } D_2$), which is much less than the extent of the radio synchrotron contours at 10.55 GHz in Fig. 2 indicate. We conclude, that the extended hard X-ray emission originates from a PWN with a photon index between $1.4 \leq \Gamma \leq 1.9$ and an unabsorbed luminosity of $L_X = 4.4 \times 10^{32} D_2^2 \text{ erg s}^{-1}$ in the 2–8 keV energy band.

4. Discussion

We can now begin to estimate some of the fundamental properties of the putative pulsar in G18.95–1.1. Using the relationship between

the spin-down energy loss rate (\dot{E}) and the non-thermal X-ray luminosity of the pulsar and the PWN (Possenti et al. 2002) of $(4.6_{-0.9}^{+4.3}) \times 10^{32} D_2^2$ erg s $^{-1}$, we estimate \dot{E} to be $(6.7_{-2.0}^{+6.4}) \times 10^{35}$ erg s $^{-1}$. Following Seward & Wang (1988), adopting an average age of G18.95–1.1 of (5300 ± 900) yr (see Harrus et al. 2004), a canonical moment of inertia of the neutron star of $I = 10^{45}$ g cm 2 , and assuming further a constant braking index of 3, that spin down happens via magnetic dipole radiation, and that the current value of the pulsar’s spin period is much larger than its initial one, the current spin period (P), the period derivative (\dot{P}), and the surface magnetic field of the pulsar is estimated to be $P = 0.4_{-0.3}^{+0.4}$ s, $\dot{P} = (1.2_{-0.8}^{+0.9}) \times 10^{-12}$ s s $^{-1}$, and $B_0 = (2.2_{-1.6}^{+1.9}) \times 10^{13}$ G, respectively. These parameters can only serve as rough estimates as they are derived from the relation between L_X and \dot{E} which can vary by about one order of magnitude (see e.g., Possenti et al. 2002). It should also be kept in mind that B_0 gives the field strength at the magnetic equator and that the field strength at the magnetic poles can be a factor of 2 higher.

If the inferred values for the period, period derivative, and magnetic field are correct, this pulsar candidate occupies a highly interesting and sparsely populated place in the $P - \dot{P}$ diagram. It would be located close to the line of the quantum critical field of $B_c = 4.4 \times 10^{13}$ G (see e.g., Kondratiev et al. 2009), which divides normal radio pulsars and the more exotic radio-quiet objects, such as the anomalous X-ray pulsars (AXP) and soft gamma-ray repeaters (SGRs).

5. Summary

We report the detection of a faint X-ray point source, CXOU J182913.1-125113, in the inner part of the composite SNR G18.95–1.1 and a trail of diffuse emission pointing towards the center of the SNR. These sources are considered to be the pulsar and its wind nebula. The best fit to the spectrum of the pulsar candidate is an absorbed powerlaw model ($\Gamma = 1.6$, $N_H = 1 \times 10^{22}$ cm $^{-2}$) with an unabsorbed luminosity in the 0.5–8 keV energy band of $L_X \simeq 4.1 \times 10^{31} D_2^2$ erg s $^{-1}$. The X-ray luminosity of the PWN ($1.4 \leq \Gamma \leq 1.9$, $N_H = 1.6 \times 10^{22}$ cm $^{-2}$) amounts to $L_X \simeq 5.4 \times 10^{33} D_2^2$ erg s $^{-1}$ in the 0.5–8 keV energy band. It appears as if the spectrum extracted from the region which contains

the PWN shows thermal emission from the SNR along the line-of-sight or the PWN has been disturbed by the reverse shock so that thermal and non-thermal emission is mixed.

Although pulsations have not been reported for the pulsar, we estimate the spin period and the period derivative to be $P = 0.4_{-0.3}^{+0.4}$ s and $\dot{P} = (1.2_{-0.8}^{+0.9}) \times 10^{-12}$ s s $^{-1}$, assuming the dipole approximation. Compared to other rotation-powered pulsars, a high magnetic field of $B_0 = (2.2_{-1.6}^{+1.9}) \times 10^{13}$ G is implied by its location in the $P - \dot{P}$ diagram. This value is close to that of the quantum critical field and makes this source a highly interesting object for follow-up observations.

Support for this work was provided by NASA through *Chandra* Award Number GO9-0081X.

REFERENCES

- Borkowski, K. J., Lyerly, W. J., & Reynolds, S. P. 2001, *ApJ*, 548, 820
- Dickey, J. M., & Lockman, F. J. 1990, *ARA&A*, 28, 215
- Fürst, E., Reich, W., Reich, P., Sofue, Y., & Handa, T. 1985, *Nature*, 314, 720
- Fürst, E., Hummel, E., Reich, W., Sofue, Y., Sieber, W., Reif, K., & Dettmar, R.-J. 1989, *A&A*, 209, 361
- Fürst, E., Reich, W., & Aschenbach, B. 1997, *A&A*, 319, 655
- Gaensler, B. M., & Slane, P. O. 2006, *ARA&A*, 44, 17
- Harrus, I. M., Slane, P. O., Hughes, J. P., & Plucinsky, P. P. 2004, *ApJ*, 603, 152
- Kondratiev, V. I., McLaughlin, M. A., Lorimer, D. R., Burgay, M., Possenti, A., Turolla, R., Popov, S. B., & Zane, S. 2009, *ApJ*, 702, 692
- Monet, D. G., et al. 2003, *AJ*, 125, 984
- Nakanishi, H., & Sofue, Y. 2003, *PASJ*, 55, 191
- Odegard, N. 1986, *AJ*, 92, 1372
- Patnaik, A. R., Velusamy, T., & Venugopal, V. R. 1988, *Nature*, 332, 136

- Petre, R., Kuntz, K. D., & Shelton, R. L. 2002, ApJ, 579, 404
- Plucinsky, P. P., Dickel, J. R., Slane, P. O., Edgar, R. J., Gaetz, T. J., & Smith, R. K. 2002, APS Meeting Abstracts, 17037
- Possenti, A., Cerutti, R., Colpi, M., & Mereghetti, S. 2002, A&A, 387, 993
- Posson-Brown, J., Grant, C., Allen, G., Plucinsky, P. P., & Edgar, R. J. 2010, <http://cxc.harvard.edu/twiki/bin/view/AcisCal/TCTIHowTo>
- Reich, W., Fürst, E., Haslam, C. G. T., Steffen, P., & Reif, K. 1984, A&AS, 58, 197
- Safi-Harb, S. 2004, Boletín de la Asociación Argentina de Astronomía La Plata Argentina, 47, 277
- Seward, F. D., & Wang, Z.-R. 1988, ApJ, 332, 199
- Smith, R. K., Brickhouse, N. S., Liedahl, D. A., & Raymond, J. C. 2001, ApJ, 556, L91
- Toscano, M., Sandhu, J. S., Bailes, M., Manchester, R. N., Britton, M. C., Kulkarni, S. R., Anderson, S. B., & Stappers, B. W. 1999, MNRAS, 307, 925
- Wilms, J., Allen, A., & McCray, R. 2000, ApJ, 542, 914